

Atomic structure of carbon nanotubes from scanning tunneling microscopy

L. C. Venema

Department of Applied Sciences and DIMES, Delft University of Technology, Lorentzweg 1, 2628 CJ Delft, The Netherlands

V. Meunier and Ph. Lambin

Departement de Physique, Facultes Universitaires Notre-Dame de la Paix, 61 Rue de Bruxelles, B-5000 Namur, Belgium

C. Dekker

Department of Applied Sciences and DIMES, Delft University of Technology, Lorentzweg 1, 2628 CJ Delft, The Netherlands

(Received 23 August 1999)

The atomic structure of a carbon nanotube can be described by its chiral angle and diameter and can be specified by a pair of lattice indices (n,m) . The electronic and mechanical properties are critically dependent on these indices. Scanning tunneling microscopy (STM) is a useful tool to investigate carbon nanotubes since the atomic structure as well as the electronic properties of individual molecules can be determined. This paper presents a discussion of the technique to obtain (n,m) indices of nanotubes from STM images in combination with current-voltage tunnel spectra. Image contrast, distortion effects, and determination of chiral angle and diameter are discussed. The procedure of (n,m) identification is demonstrated for a few single-walled carbon nanotubes.

I. INTRODUCTION

Carbon nanotubes¹ are hollow cylindrical molecules that have unique electronic² and mechanical³ properties. They can be considered as graphene sheets that are rolled up into seamless cylinders (Fig. 1). Each nanotube can be specified by a pair of indices (n,m) that corresponds to a specific chiral angle ϕ and diameter d . Remarkably, nanotubes can be either semiconducting or metallic, which depends critically on the (n,m) numbers.² These indices can in principle be obtained experimentally by measuring both ϕ and d from either transmission electron microscopy (TEM) and diffraction⁴ or by scanning tunneling microscopy (STM).^{5,6} STM appears to be more suitable to probe individual molecules. Topographic imaging can be combined with tunneling spectroscopy measurements.⁵⁻⁸ This is a powerful technique since the predicted relation between atomic and electronic structure can be tested. STM measurements indeed confirmed that nanotubes can be either semiconducting or metallic, depending on the chirality and diameter.^{5,6}

This paper presents a discussion of (n,m) identification for individual nanotubes by use of STM measurements. Section II explains how the atomic structure of a nanotube can be described by a pair of (n,m) lattice indices. Section III gives the experimental details of the STM measurements. Section IV explains how ϕ and d are determined from images and current-voltage tunnel spectra. Also, the lattice contrast is discussed together with a number of distortion effects that have to be taken into account. Section V describes the identification of two different nanotubes, a semiconducting and a metallic example. The atomically resolved STM images of these nanotubes are compared to calculated images. Section VI gives a summary of the results.

II. DEFINITION OF NANOTUBE INDICES

As shown in Fig. 1, a carbon nanotube can be thought of as a cylinder constructed from a graphene sheet. A vector \mathbf{C}

is defined pointing from one carbon site to another equivalent site in the hexagonal lattice. By cutting out the sheet along the dashed lines perpendicular to \mathbf{C} and wrapping up the sheet in the direction of the vector, a seamless cylinder

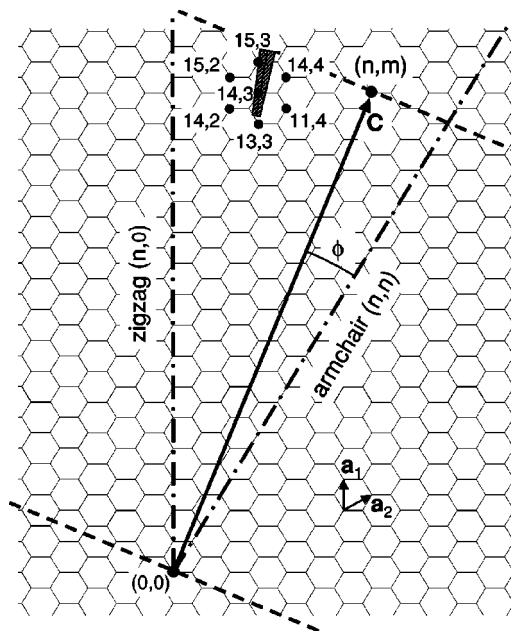


FIG. 1. A graphene sheet that can be rolled up into a single-walled nanotube by cutting out the sheet along the dashed lines and rolling the sheet up along vector \mathbf{C} . \mathbf{a}_1 and \mathbf{a}_2 are the unit vectors of the graphene lattice. The dash-dotted lines denote the main symmetry directions in the graphene sheet, $(n,0)$ and (n,n) , or, the zigzag and armchair directions respectively. Also shown are (n,m) indices around $(14,3)$. The corresponding ϕ , d and electronic behavior for the nanotubes with these (n,m) indices are given in Table I. The hatched trapezium represents a measurement of ϕ and d for nanotube 2 in Fig. 4. The half widths of this area are the measurement errors.

TABLE I. (n,m) indices with the corresponding chiral angles, diameters, and electronic behavior for the seven nanotubes indicated in Fig. 1.

(n,m)	d (nm)	ϕ ($^\circ$)	Electronic behavior
(13,3)	1.15	19.8	Semiconductor
(14,2)	1.18	23.4	Metal
(13,4)	1.21	17.0	Metal
(14,3)	1.23	20.5	Semiconductor
(15,2)	1.26	23.8	Semiconductor
(14,4)	1.28	17.8	Semiconductor
(15,3)	1.31	21.1	Metal

can be obtained, with diameter $d=|\mathbf{C}|/\pi$. The vector \mathbf{C} can be related to the unit vectors \mathbf{a}_1 and \mathbf{a}_2 as $\mathbf{C}=n\mathbf{a}_1+m\mathbf{a}_2$. The pair of indices (n,m) defines the nanotube. The corresponding chiral angle ϕ and diameter d are

$$\phi = \arccos\left[\frac{\sqrt{3}(n+m)/2}{\sqrt{n^2+m^2+nm}}\right]$$

$$d = \frac{a}{\pi}\sqrt{n^2+m^2+nm},$$

where $a=0.246$ nm is the lattice constant. $(n,0)$ and $(0,n)$ denote special symmetry directions in the graphene lattice, named respectively zigzag and armchair (dash-dotted lines in Fig. 1). They differ by an angle of 30° . A sheet rolled up along one of these lines results in a nonchiral tube, with $\phi=0^\circ$ for an armchair and $\phi=30^\circ$ for a zigzag nanotube.

Nanotubes can be either semiconducting or metallic. The general rule is that nanotubes are metallic when $(n-m)$ is a multiple of 3 and semiconducting otherwise.² As an example, Table I lists a few nanotubes with indices around (14,3), which are also indicated in Fig. 1. This table shows that a high accuracy is required in both the measured diameter and the chiral angle to distinguish between two nanotubes with neighboring (n,m) indices. (14,3) and (15,3) for example differ only 0.08 nm in diameter and 0.6° in chiral angle. A measurement of the electronic behavior can be conclusive in this case, since the first is a semiconductor while the latter is a metal.

III. EXPERIMENTAL DETAILS

The measurements discussed in this paper were performed on carbon nanotubes on a Au(111) surface. Nanotubes were synthesized by laser evaporation (material provided by R. E. Smalley and coworkers.⁹) TEM images show that this material consists mainly of single-walled nanotubes with a diameter of about 1.4 nm. Au(111) was prepared by flash-heating a piece of about 30 mm^3 from a 99.99% pure gold wire. The single-crystalline facets appearing on the surface after cooling were used as substrates. Nanotube soot was dispersed in dichloroethane and treated in an ultrasonic bath to unravel the material into nanotube bundles and single nanotubes. A droplet of the dispersion was then deposited on the Au(111) substrates in ambient conditions.

All measurements were done in an STM operated in constant-current mode at 4 K. STM tips were mechanically cut from a Pt(90%)Ir(10%) wire. Typical tunneling param-

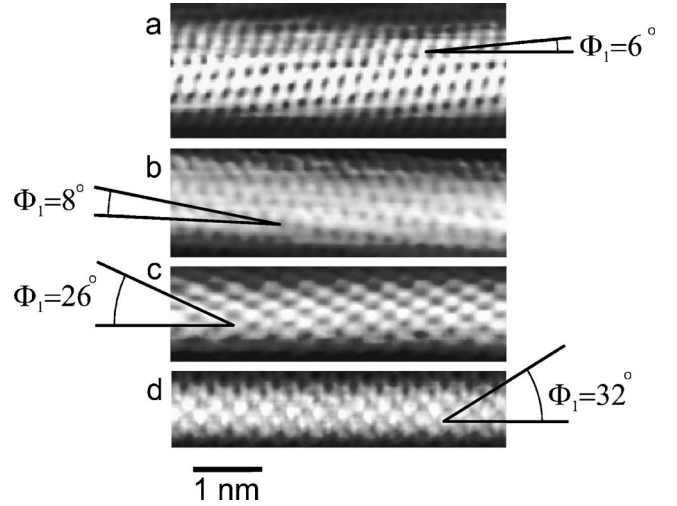


FIG. 2. STM images of atomically resolved carbon nanotubes. For each nanotube the apparent angle ϕ_1 between hexagon rows and the tube axis is indicated. The 1-nm bar indicates the scale for all four images. (a)-(b) Two chiral nanotubes with small chiral angles. (c)-(d) Two chiral nanotubes with large chiral angles (near 30°).

eters were 60 pA and 0.1 V. Current-voltage ($I-V$) tunnel spectra on the nanotubes were taken by switching off the feedback and recording the current I as a function of the bias voltage V applied to the sample. The differential conductance dI/dV calculated from the $I-V$ spectra is roughly proportional to the density of states (DOS) of the sample. For large voltage ranges ($\geq \pm 1$ V) dI/dV is usually normalized by dividing by I/V to account for the voltage dependence of the tunnel barrier.¹⁰ We used this normalization method to analyze our spectroscopy data.

IV. STM DATA ANALYSIS

This section discusses methods to obtain the chiral angle ϕ and diameter d from STM measurements of carbon nanotubes. Part A of this section discusses the apparent lattice contrast in the STM images of carbon nanotubes. Often a nonhexagonal lattice is observed which can be attributed to various effects. Furthermore, the apparent chiral angle is distorted due to the cylindrical shape of nanotubes. Part B describes a procedure to cancel out the distortion and obtain the true chiral angle ϕ . In part C, methods to obtain the diameter d are discussed.

A. Atomic contrast in STM imaging

Figure 2 shows various examples of atomically resolved STM images of chiral carbon nanotubes with apparent chiral angles ϕ indicated. Typically, STM images of nanotubes do *not* show a hexagonal configuration of carbon atoms. Instead, a triangular lattice of dark and white dots is usually observed as seen for example in Figs. 2(c) and 2(d). For graphite, various effects are known that can distort the expected hexagonal pattern. The *ABAB* stacking sequence of the three-dimensional-layered structure in graphite results in two inequivalent atomic sites in each unit cell, which leads to an asymmetry in STM images.¹¹ Obviously, this can be ruled out for single-walled carbon nanotubes. There are however

also a number of tip-related effects that can explain the distortion of the hexagonal graphene lattice.^{12,13} The geometrical shape of the tip and the type of electronic orbitals protruding from the tip apex play an important role in the apparent contrast of the lattice. Mizes *et al.*¹² argued that the STM image of a hexagonal lattice is built up by three independent Fourier components of equal magnitude. Imaging with a multiatom tip leads to a superposition of several images, where the three components that make up the total image are not equal. This can explain various anomalous images that have been observed for planar graphite, such as triangular or striped patterns. The same effect may play a role in imaging the graphene lattice of carbon nanotubes.

Recently, Kane and Mele discussed a mechanism of symmetry breaking in carbon nanotubes that would even occur in an ideal tunneling experiment with a perfect single-atom tip.¹⁴ Due to scattering of electrons at defects or ends of nanotubes, STM images may contain interference patterns. Kane and Mele showed for example that large momentum backscattering in armchair tubes leads to a modulation into a $\sqrt{3} \times \sqrt{3}$ pattern, whereas a small momentum backscattering may give striped patterns.

Another effect that distorts the hexagonal lattice in nanotubes is the curvature of the surface. The overlap between the external lobes of the π orbitals on neighboring carbon atoms decreases due to the curvature, except for the bonds parallel to the nanotube axis (as in zigzag nanotubes). It therefore turns out that for a nanotube with a chiral angle near $\phi=30^\circ$, the bonds parallel or almost parallel to the tube axis are imaged as protrusions, which leads to the typical triangular pattern of white dots. When $\phi \approx 0^\circ$ (close to armchair), there are no bonds parallel to the axis and the lattice should appear more hexagonal. The nanotubes in Figs. 2(a) and 2(b) are near armchair and indeed have a more hexagonal contrast than the near-zigzag nanotubes in Figs. 2(c) and 2(d), where the white protrusions are the most prominent features.

B. Chiral angle

All the mechanisms described above can have an effect on the lattice contrast but do *not* distort the chiral structure of a nanotube. STM images can thus be used to determine the chirality. However, the geometrical configuration of the STM tip tunneling on a cylindrical structure [Fig. 3(c)] does lead to an overestimation of the value for the chiral angle. This effect was first noted by Ge *et al.*,¹⁵ and discussed in detail by Meunier *et al.*¹⁶ Figure 3(c) illustrates the distortion mechanism. A nanotube with radius r lies on a substrate in the xy plane with its axis in the x direction. The tunnel distance h is kept constant while the tip scans in constant-current mode. The shortest tunnel path from the tip to the tube is perpendicular to the substrate only when the tip is exactly on top of the tube. In general, the tunnel current flows to the side of the nanotube and the atom at site (x,y,z) on the nanotube surface will therefore be projected in the STM image at $[x,(1+h/r)y,z]$. Effectively, the hexagonal lattice is stretched by a factor of $(1+h/r)$ in the y direction, transverse to the tube axis. This effect can be considerable; for a typical tunneling distance h of 0.4 nm and a tube radius of 0.7 nm, the lattice is distorted by $\sim 60\%$.

This distortion is apparent from the angle between zigzag and armchair directions in the STM images. For example,

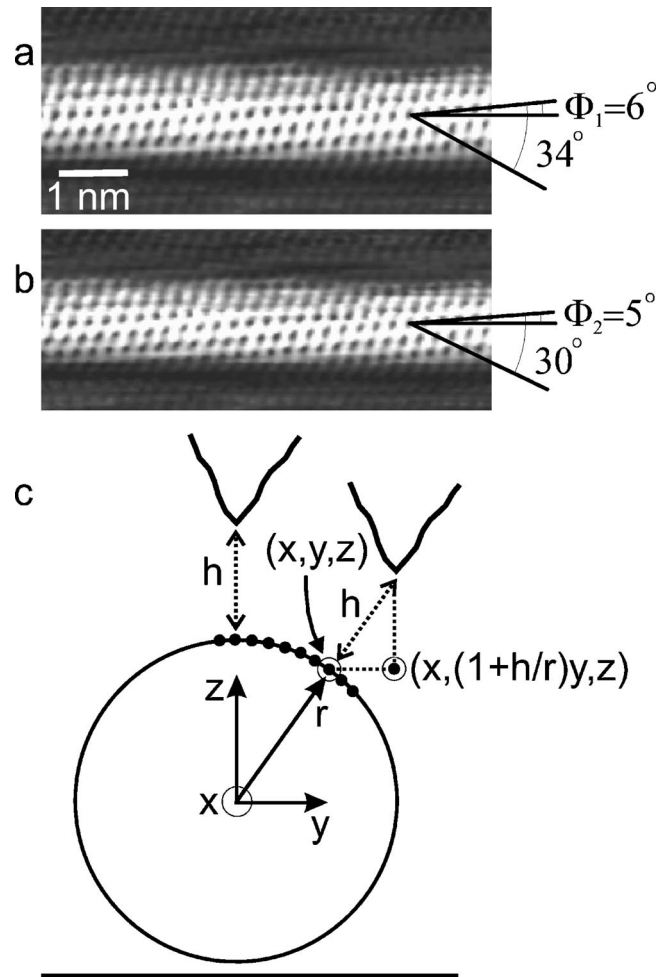


FIG. 3. Illustration of the image distortion mechanism for nanotubes and a correction method. The 1-nm bar indicates the scale for both images in (a) and (b). (a) An uncorrected image with an angle between armchair and zigzag directions of 34° instead of 30° . This is attributed to a distortion effect, which stretches the atomic lattice in the direction perpendicular to the tube. The apparent angle $\phi_1 = 6^\circ$. (b) The same image as (a), corrected for the distortion. This is done by decreasing the image in the perpendicular direction to obtain a 30° difference between the zigzag and armchair directions. A chiral angle $\phi_2 = 5^\circ$ is determined from this corrected image. (c) A sketch illustrating the geometrical distortion mechanism. A nanotube with radius r lies in the xy plane with its axis in the x direction. When the STM tip tunnels to the side of the nanotube, an atom at position (x,y,z) is projected in the STM image at $[x,(1+h/r)y,z]$.

Fig. 3(a) is an uncorrected image where the angle between zigzag and armchair directions is higher, 34° , than it should be (30°). This is due to a stretching of the lattice in the direction normal to the tube axis. The angle $\phi_1 = 6^\circ$ seen in this image is therefore not equal to the true chiral angle. To determine the true chirality, the image size is reduced in the direction normal to the nanotube axis until the angle between the zigzag and armchair rows fits to 30° , to compensate for the asymmetric inflation. Figure 3(b) shows the STM image after such a correction, from which a chiral angle $\phi_2 = 5^\circ$ is found. By carrying out this procedure for various armchair-zigzag angles along the nanotube a $\phi_1 = 6.2 \pm 0.4$ is obtained. This angle is 32% higher than the ϕ_2 of $4.7 \pm 0.4^\circ$ from the

corrected image. The distortion found for various nanotubes from STM images varies between 15% and 70%.

Clauss *et al.*¹⁷ discussed a distortion mechanism for the chiral angle that is not related to the STM configuration but to the geometry of a nanotube within a rope. When packed within a rope, nanotubes may be twisted. Atomically resolved STM images of ropes indeed show twisted tubes.¹⁷ The measured angle of the lattice with respect to the nanotube axis in that case is not only related to the nanotube chirality, but also to the twist angle. We do not include this effect in the analysis of our STM images. It is unlikely that individual nanotubes separated from ropes remain twisted, because large twisting angles are energetically very unfavorable for individual nanotubes.¹⁸ Furthermore, the energy gap in the DOS predicted to be induced by the twist is not observed in our STM spectra.

C. Diameter

The diameter of a nanotube can be obtained from a line profile perpendicular across the nanotube. The major distortion that influences the apparent tube width in such a profile arises from the geometrical convolution between the nanotube and the STM tip shape.¹⁹ The nanotube diameter can in principle be measured from the apparent width by careful deconvolution of the tip shape. This method can be used if ultrasharp tips are available. In general however, it is hard to obtain an accurate value for the diameter since the radius of curvature of an STM tip is typically ~ 10 nm, i.e., more than one order of magnitude larger than the tube radius.

Alternatively, the diameter can be estimated from the height of the nanotube relative to the substrate. The van der Waals distance between the substrate and the tube, about 0.25 nm,²⁰ then has to be taken into account. Furthermore, because of differences in electronic structure, the tunnel distances are not necessarily the same on the nanotube and the gold substrate. Since the tube height is measured relative to the substrate this difference in tunnel distances may lead to an error in the diameter. *Ab initio* calculations by Rubio²¹ show however that the error in diameter due to this effect will be less than 1%. A more substantial error in the apparent height may arise from mechanical deformation of the nanotube. A small deformation also may arise from the van der Waals forces between the substrate and the nanotube. For an armchair nanotube with a diameter of about 1.4 nm this deformation is calculated to be only 2%.²² As is noticed below, the typical tunnel distances appear to be small, which implies that the STM tip may exert significant forces on the nanotube. This may lead to compression of nanotubes during imaging and consequently to anomalous low apparent heights (see Sec. V).

Yet another way to obtain the diameter is to determine the tunneling DOS for a nanotube. Both semiconducting and metallic nanotubes have a DOS consisting of a series of one-dimensional energy subbands.^{23,24} The separation between the band edges depends on the diameter. Figure 4(c) shows examples of STM spectra obtained for a semiconducting (1) and a metallic (2) nanotube. The band-edge separations are indicated in the figure by ΔE_{sub} . For semiconducting tubes this separation is an energy gap of width $\Delta E_{sub} = 2d_{nn}\gamma_0/d$, where d_{nn} is the nearest-neighbor distance between carbon atoms, 1.42 Å, and γ_0 is the π - π energy

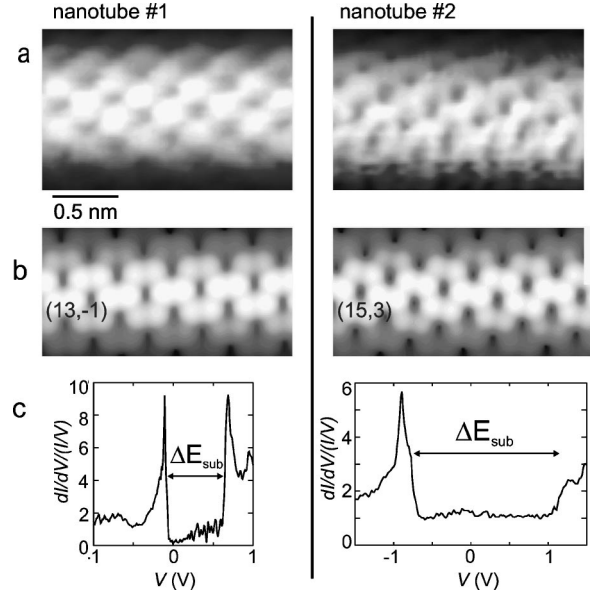


FIG. 4. STM images and tunnel spectra for two different carbon nanotubes. The 0.5-nm bar indicates the scale for all four images in (a) and (b). (a) Atomically resolved STM images of two nanotubes 1 and 2. (b) Two calculated images based on the (n,m) indices that are found for the nanotubes shown in (a). (c) Normalized dI/dV spectra for these nanotubes. Nanotube 1 appears to be semiconducting whereas nanotube 2 is metallic. Band edge separations ΔE_{sub} are indicated for both curves.

overlap between neighboring atoms. Metallic nanotubes have a plateau of constant DOS between subbands of $\Delta E_{sub} = 6d_{nn}\gamma_0/d$. A theoretical value for γ_0 of 2.5 eV has been estimated by Mintmire *et al.* using a first-principles local-density approximation (LDA) to calculate the band structure of armchair carbon nanotubes.²⁵ This type of calculations however typically give a 10-20 % too small value. In a recent review paper a value of 2.9 ± 0.2 eV was concluded to be the best estimate for γ_0 from a critical evaluation of various theoretical and experimental results.²⁶ In this paper we determined the diameter both from the apparent height and by measuring ΔE_{sub} using this value of $\gamma_0 = 2.9 \pm 0.2$ eV.

V. DISCUSSION OF THE (n,m) IDENTIFICATION

Two examples are shown of nanotubes for which the (n,m) indices are identified. Figure 4(a) shows atomically resolved STM images of these two nanotubes, which both are chiral. Tunneling spectra that were taken on these tubes are shown in Fig. 4(c). From these spectra nanotube 1 can be identified as a semiconductor and nanotube 2 as a metallic tube. Table II lists the parameters obtained from the STM analysis done for these nanotubes. Diameters are obtained by two methods, described in Sec. IVC, from the apparent height and from the subband separations. The chiral angles ϕ_2 are obtained from the corrected atomically resolved images, following the procedure described in Sec. IVB. From this correction procedure we find distortions of about 15% for nanotube 1 and 60% for nanotube 2. These distortions give a tunnel distance h of respectively ~ 0.1 and ~ 0.4 nm, using the formula for distortion $(1+h/r)$ which follows from the simple picture of Fig. 3(c). These values indicate

TABLE II. The results from data analysis of the STM measurements on the two nanotubes shown in Fig. 4(a). ΔE_{sub} is the separation between subbands and $d_{\Delta E_{sub}}$ is the diameter that is calculated from this energy difference using $\gamma_0 = 2.9 \pm 0.2$ eV. d_h is the diameter estimated from the apparent height of the nanotubes. The true chiral angle ϕ_2 is measured from corrected STM images. Also given are (n,m) indices with their corresponding ϕ_t and d_t that fit to the experimentally obtained values. The electronic behavior for the nanotubes with these (n,m) numbers is indicated in the last column.

Tube	ΔE_{sub} (eV)	$d_{\Delta E_{sub}}$ (nm)	d_h (nm)	ϕ_2 ($^\circ$)	(n,m)	d_t (nm)	ϕ_t ($^\circ$)	Electronic behavior
1	0.80 \pm 0.05 Semiconductor	1.0 \pm 0.1	0.7 \pm 0.1	25 \pm 1	(12,-1)	0.90	25.7	Semiconductor
					(13,-1)	0.98	26.0	Semiconductor
					(14,-1)	1.06	26.3	Metal
2	1.95 \pm 0.05 Metal	1.27 \pm 0.09	0.7 \pm 0.1	20 \pm 1	(14,3)	1.23	20.5	Semiconductor
					(15,3)	1.31	21.1	Metal

that the STM tip is close to the nanotube and in the case of the first tube even in contact. In view of these small values it is likely that the nanotubes are compressed during imaging due to the forces exerted by the STM tip. The effective stretching of the image perpendicular to the nanotube axis probably deviates from $(1+h/r)$ due to a tip shape that is more complicated than a single atom and possibly also because of the compression of the nanotubes by the STM tip. The procedure to obtain the correct chiral angle by decreasing the image in the y direction is independent of the exact amount of stretching however.

The apparent height method yields anomalously small values for the diameter d_h , which is most likely due to the above-mentioned flattening of the nanotubes by the STM tip during imaging. This method thus appears to be unreliable. We instead determine the diameters $d_{\Delta E_{sub}}$ found from the subband separations in the DOS. The experimental results for both nanotubes are compared in Table II to theoretical values of ϕ_t and d_t calculated for nanotubes with indices (n,m) yielding the best fits. The error in determining the chiral angle is typically $\sim 1^\circ$. The error in the diameter is ~ 0.1 nm and is mainly determined by an uncertainty in γ_0 . The measurement uncertainty area is indicated for nanotube 2 as the hatched area in Fig. 1. For nanotube 1, (12,-1), (13,-1), and (14,-1) fit to the observed chirality and diameter. However, (14,-1) can be ruled out as a possibility since nanotube 1 is semiconducting. Nanotube 2 fits to (14,3) and (15,3), as can also be seen in Fig. 1, but, since it is metallic, (15,3) can be singled out as the only candidate. In general, fitting the indices for metallic nanotubes is somewhat easier since only one third of all possible (n,m) nanotubes is metallic.

The experimental images are compared to calculated images in Fig. 4(b) for nanotubes with indices (13,-1) and (15,3). These calculations are done by using a tight-binding π -electron Hamiltonian as described by Meunier *et al.*¹⁶ The tip was taken as a single atom with an s orbital, as in the Tersoff-Hamann theory,²⁷ and the corresponding tip density of states was assumed to have a Gaussian shape. Input parameters for these calculations are the (n,m) numbers and the tunnel distance h between the STM tip and the nanotube.

The calculated images in Fig. 4(b) show the remarkable result that the lattice contrast deviates considerably from a hexagonal lattice, even for a perfect single-atom tip. Comparing the experimental images to these calculations, good resemblances are observed. The most prominent features for the near-zigzag nanotube 1 are the white protrusions, which also appear clearly in the calculated images. The rectangular shape of these protrusions does not come out very clearly in the STM images. It may be expected however that the detailed structure will be influenced by the STM tip shape.

VI. SUMMARY

It has been demonstrated that the (n,m) indices for a specific nanotube can be identified from STM measurements by measuring both the chiral angle and the diameter. The chiral angle ϕ is determined from atomically resolved images. These images have to be corrected to account for a geometric distortion that otherwise show 15-70 % overestimated chiral angles. Diameters d can be obtained from the tunneling DOS, since the energy subband separations are related to the diameters. Two nanotubes, one semiconducting and one metallic, were presented as examples for which ϕ and d were obtained. For both nanotubes, (n,m) indices could be found that fit to the experimentally determined ϕ and d and electronic behavior. We conclude that, within the uncertainty of the measurements which is 1° for ϕ and 0.1 nm for d , it is indeed possible to obtain accurate fits of the (n,m) indices.

ACKNOWLEDGMENTS

We thank J. Janssen, S. Lemay, J. Wildöer, and A. Rubio for help and discussions and L. Kouwenhoven for support. The work at Delft was supported by the Dutch Foundation for Fundamental Research of Matter (FOM). The work at Namur was partly performed under the auspices of the inter-university research program on Reduced Dimensionality Systems (Contract No. PAI-IUAP N. P4/10) initiated by the Belgian Federal OSTC. V.M. acknowledges a grant from the Belgian Fund for Industrial and Agricultural Research (F.R.I.A.).

- ¹C. Dekker, Phys. Today, **52** (5), pt. 22 (1999).
- ²R. Saito, G. Dresselhaus, and M. Dresselhaus, *Physical Properties of Carbon Nanotubes* (Imperial College Press, London, 1998).
- ³M. Nardelli, B. Yakobson, and J. Bernholc, Phys. Rev. Lett. **81**, 4656 (1998).
- ⁴S. Iijima and T. Ichihashi, Nature (London) **363**, 603 (1993).
- ⁵J. Wildoer, L. Venema, A. Rinzler, R. Smalley, and C. Dekker, Nature (London) **391**, 59 (1998).
- ⁶T. Odom, J.-L. Huang, P. Kim, and C. Lieber, Nature (London) **391**, 62 (1998).
- ⁷A. Hassanien, M. Tokumoto, Y. Kamazawa, H. Kataura, Y. Maniwa, S. Suzuki, and Y. Achiba, Appl. Phys. Lett. **73**, 3839 (1998).
- ⁸P. Kim, T. Odom, J.-L. Huang, and C. Lieber, Phys. Rev. Lett. **82**, 1225 (1999).
- ⁹A. Thess, R. Lee, P. Nikolaev, H. Dai, P. Petit, J. Robert, C. Xu, Y. Hee Lee, S. Gon Kim, A. G. Rinzler, D. T. Colbert, G. E. Scuseria, D. Tománek, J. E. Fischer, and R. E. Smalley, Science **273**, 483 (1996).
- ¹⁰J.A. Stroschio and R.M. Feenstra, in *Scanning Tunneling Microscopy*, edited by J.A. Stroschio and W.J. Kaiser, Methods in Experimental Physics, Vol. 27 (Academic Press, San Diego, 1993), Chap. 4, and references therein.
- ¹¹D. Tománek, S. Louie, H. Mamin, S. Abraham, R. Thomson, E. Ganz, and J. Clarke, Phys. Rev. B **35**, 7790 (1987); I. Batra and S. Ciraci, J. Vac. Sci. Technol. A **6**, 313 (1988).
- ¹²H. Mizes, S. Park, and W. Harrison, Phys. Rev. B **36**, 4491 (1987).
- ¹³M. Tsukada and K. Kobayashi, J. Vac. Sci. Technol. A **8**, 160 (1990).
- ¹⁴C. Kane and E. Mele, Phys. Rev. B **59**, R12 759 (1999).
- ¹⁵M. Ge and K. Sattler, Appl. Phys. Lett. **65**, 2284 (1994).
- ¹⁶V. Meunier and Ph. Lambin, Phys. Rev. Lett. **81**, 5888 (1998).
- ¹⁷W. Clauss, D. Bergeron, and A. Johnson, Phys. Rev. B **58**, R4266 (1998).
- ¹⁸A. Rochefort, Ph. Avouris, F. Lesage, and D. R. Salahub, Phys. Rev. B **60**, 13 824 (1999).
- ¹⁹G. Mark, L. Biro, and J. Gyulai, Phys. Rev. B **58**, 12 645 (1998).
- ²⁰A. Rubio, Appl. Phys. A: Mater. Sci. Process. **68**, 275 (1999).
- ²¹A. Rubio (private communication).
- ²²T. Hertel, R. Walkup, and Ph. Avouris, Phys. Rev. B **58**, 13 870 (1998).
- ²³J. Mintmire and C. White, Nature (London) **394**, 29 (1998).
- ²⁴J.-C. Charlier and Ph. Lambin, Phys. Rev. B **57**, R15 037 (1998).
- ²⁵J. Mintmire and C. White, Appl. Phys. A: Mater. Sci. Process. **67**, 65 (1998).
- ²⁶G. Dresselhaus, M. Pimenta, R. Saito, J.-C. Charlier, S. Brown, P. Corio, and M. Dresselhaus (unpublished).
- ²⁷J. Tersoff and D. Haman, Phys. Rev. Lett. **50**, 1998 (1983).